MECHANICS AND CONTROL
Vol. 30 No. 4 2011

V. RIMŠA*, R. KAČIANAUSKAS*, H. SIVILEVIČIUS**

FINITE ELEMENT SIMULATION OF THE NORMAL INTERACTION OF PARTICLES IN THE VISCO-ELASTIC SOLID

SUMMARY

This paper addresses the 3D FE simulation of the normal interaction of stiff but deformable particles in binder matrix on the meso-scale. The particles are assumed to be elastic spheres while matrix is considered as viscoelastic solid. The investigation is aimed to capture interaction in terms of normal forces under tension. The problem is considered by applying geometrically linear and nonlinear approaches. Results illustrate influence of initial inter-particle gap reduction of which yields significant increase of the interaction force. Comparison between purely elastic and viscoelastic solutions is also presented.

Keywords*: particles, geometric nonlinearity, viscoelastisity, normal interaction force, interface layer*

SYMULACJA ODDZIAŁYWANIA CZĄSTEK ZE SPRĘŻYSTO-LEPKIM OŚRODKIEM METODĄ ELEMENTÓW SKOŃCZONYCH

Niniejszy artykuł dotyczy trójwymiarowej symulacji metodą elementów skończonych oddziaływania w kierunku normalnym sztywnych, ale odkształcalnych cząstek w spoistej osnowie na poziomie mezoskopowym. Cząstki są traktowane jako sprężyste kule, zaś osnowa jako ciało lepkosprężyste. Badania mają na celu znalezienie sił oddziaływania pod obciążeniem. Zagadnienie jest rozpatrywane przy zastosowaniu modelu geometrycznie liniowego i nieliniowego. Wyniki pokazują wpływ wstępnego zmniejszenia odstępu na znaczący wzrost siły oddziaływania. Przedstawione jest również porównanie między rozwiązaniem sprężystym i lepkosprężystym.

Słowa kluczowe*: cząstki, nielinowość geometryczna, lepkosprężystość, oddziaływanie w kierunku normalnym, warstwa graniczna*

1. INTRODUCTION

Majority of real engineering materials are heterogeneous and multicomponent mixtures, separate components of which possess large diversity of properties on various scales of heterogeneity. Evaluation of mechanical behaviour of them has been the focus of much research over the last decades and various theories and approaches of different complexity are used for characterization purposes.

From the point of view of mechanics the material is regarded as heterogeneous solid. We restrict to particular case of the solid, heterogeneity of which is caused by stiffer particles of different size and properties being the inclusions dispersed in a softer solid matrix. Asphalt-type materials and polymer materials containing coarse aggregates and soft matrix may be regarded as representative prototype of this model. In the case of asphalt, coarse aggregates are stone particles of various shapes and sizes being irregularly distributed in space. The matrix (including binder and fine aggregates) possesses very complex temperature, time and rate dependent behaviour.

Since detailed review is beyond of our purposes, the most characteristic approaches employed for development of deterministic simulation models and selected samples will be mentioned.

In a purely engineering approach, asphalt-type materials are regarded as representative sample. Mechanical behaviour of them is characterized by gradual change of their properties in time under loading. Permanent deformation is one of the considerable load-associated distress types affecting the performance of asphalt mixtures. Comprehensive review on evaluation of mechanical properties is given by [1] and references herein. The mechanistic-empirical approach couples the mechanistic computations with the empirical predictions and the mixture content. The overall accuracy of the mechanistic-empirical models heavily relies upon the quantity and quality of the empirical data used for calibrating of the empirical model. Nevertheless, this approach is widely used in engineering area and various sophisticated models relating macroscopic parameters with composition of particles has been developed.

The use of constrained and unconstrained optimization models in gradation design of hot mix asphalt mixture by Sivilevičius *et al.* [2] and stochastic optimization by Alavi *et al.* [1] are referred for the sake of illustration.

Contrary to the engineering empirics, the continuum mechanics based approach provides another alternative. Significant efforts have been made recently, in development of macroscopic models for time-dependent solids. These models are able to capture various viscos and coupled effects in homogenised mixtures or binder components. The Schapery's single integral model has been widely used to characterize the nonlinear viscoelastic behaviour of engineering materials [3]. Review of viscoelastic models is given in [4]. Example of viscoplastic approach to asphalt concretes is presented in [5]. The viscous models coupled

* Vilnius Gediminas Technical University, Sauletekio Ave. 11, 10223 Vilnius; e-mail: vrimsa@hotmail.com; rkac@fm.vgtu.lt
** Vilnius Gediminas Technical University, Plytines St. 27, 10223 Vilnius; e-mail: henrikas.sivilevicius@vgtu.lt

with continuum damage were considered in [6, 7]. An advanced method for determining fatigue-damage resistance characteristics of asphalt at low temperatures employing fundamentals of viscoelastic continuum damage mechanics is presented by Mun and Lee [8]. Most of the above studies carried out on constitutive modelling of mixtures were based on phenomenological models of solids. Alternative approach based on a rate type viscoelastic fluid model with incorporated multiple relaxation mechanisms was considered in [9].

Many research studies have been performed in the past decade in order to understand the role of various constituents for macroscopic behaviour of these particulate solids by means of numerical simulation. Because of the high heterogeneity, the routine application of the conventional Finite Element (FE) method using continuum elements poses serious difficulties. Consequently, numerical modelling is shifted towards microstructure effects and the Discrete Element (DE) method is recently in progress. Conceptually, by applying the DE technique a solid body is treated as a system of interacting particles. Macroscopic model comprises particles being connected by deformable elements. Behaviour of connecting elements is characterized by the constitutive interaction laws and described in terms of the force-displacement relationships.

A comprehensive review of the latest developments in the field of mix compositions and asphalt concrete in particular is recently presented by Liu *et al*. [10]. This review overwhelms the most important findings published during the last decade and addresses advances in understanding role of mixture characteristics and their impact on mechanical behaviour of mixtures. Three types of problems concerning the experiment-based methods, multiphase micromechanical models and numerical models were reviewed. The review involves numerical models started their applications in the early 1990s and includes both the FE and DE methods.

Two types of approaches, namely the user-made models and the image-based models were typically utilised to build numerical models. The image-based models could be captured from a digital camera, a digital scanner or X-ray computer tomography and converted to FE or DE structures. Details of these three aforementioned imaging methods with application to the generation of the FE meshes are described by Kose *et al*. [11]. The latest developments on application to FE are discussed by Dai [12] while application to DEM by You and Adhikari [13].

The major advantage of the image-based models is relatively accurate representation of the microstructure but their sample-dependent nature may be considered as principal disadvantage. User-made models are recommended by authors of the review [10] for fundamental research.

The examples of the user-made models may be found in [14–19].

Comparison of the FE and the DE approaches discovered their advantages and disadvantages.

The strength of the FEM is existence of complex viscoelastic-viscoplastic constitutive models which can simulate the time-dependent behaviour of continuum. By contrast, the advantages of DE models are that they are conceptually closer to the nature of particulate solids. The main disadvantage may be attributed to description of matrix in a framework of the DE model which is still basically restricted by elastic models.

In spite of extensive research, knowledge about contribution of particular factors to mechanical behaviour of mixtures is not satisfactory. Our investigation addresses the behaviour of the viscoelastic interface between stiffer particles under normal tension loading on the meso-scale. The most attention was focussed towards the role of initial gap to normal tension behaviour. The above problem presents a part of complex issue in development of connecting elements to build efficient but reliable simplified discretisation DE type models.

The paper is organized as follows. The problem is formulated in Section 2, where basic data are also described. The finite element model and its evaluation are given in Section 3. Numerical results and influence of various factors are discussed in Section 4. Final conclusions are drawn in Section 5.

2. PROBLEM DESCRIPTION

2.1. Modelling concept

The approach employed hereafter assumes coarse aggregated mixture as bi-material solid. The particles are assumed to be elastic spheres while the binder matrix is considered as viscoelastic solid. This paper addresses the simulation of the normal interaction under tension on the meso-scale, i.e. on the scale of aggregate, while emphasis is given on evaluation of the size of initial gap between particles.

Evaluation of the interaction may be done in various ways. In our case, the interaction is considered by conducting numerical experiment by applying 3D FEM. Thereby, displacement-driven approach is used to calculate the normal interaction force- displacement relations and stiffness.

2.2. Model description

A pair of elastic spherical particles glued by an interface material is considered hereafter. Actually, the space between and around the particles is fulfilled by viscoelastic binder material. Interaction of two particles is restricted to normal tension. Characterization of the normal interaction is done by considering particles motion in representative volume of the solid. Consequently, this volume is used as the computational domain of numerical model. In our case, geometry of computational domain is presented in a form of circular cylinder containing interacting spheres. Geometry of the central section of computational model is shown in Figure 1.

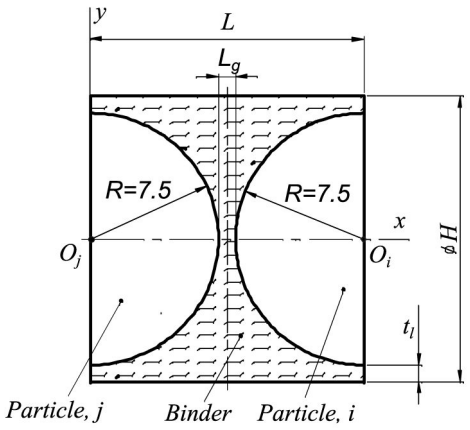

Fig. 1. Geometry of the model

Geometry of the deformable spheres i and j is defined with the radius R. The location of spheres is characterized by the central points O_i and O_j referring to local Cartesian coordinates $Oxyz$ where axis Ox points the direction between sphere's centres. Thus, the centres of spheres are defined by the coordinates x_i and x_j, respectively.

Location of the cylinder is related to spheres. It is defined by points O_i and O_j where cylinder axis coincides local coordinate axis Ox. The initial distance between surfaces of interacting spheres is denoted by L_g.

Geometry of the model cylinder is defined by its length L and diameter H. It should be clarified that the choice of the cylindrical shape of the interface model is extensively explored in simulations. In the case of bonded granular materials, see Jiang *et al*. [20], application of the cylinder is quite natural approximation of the bond. Therewith, the cylinder diameter H is restricted to minimal diameter of interacting particles. It is obvious that deformation behaviour of particles in weaker continuum is slightly different. We can refer to results exhibited by Chareyre *et al*. [21], where detailed analysis of the viscous flow induced forces acting on the solid particles in dense sphere packing was presented. It was demonstrated that in presence of neighbour particles the reprehensive volume presents composition of tetrahedrons which may approximated by cylindrical volumes.

We focus on mutual interaction of particles. Thus, the length of the imaginary cylinder L reflects the size of the particle's radius and the interface gap L_g, $L = 2R + L_g$. The cylinder diameter H also depends on the particle's radius and the thickness of artificially introduced outer cylindrical shell-type layer having thickness t_l, $H = 2(R + t_l)$. Presence of this layer gives more freedom to particles motion in the cylinder model and helps to avoid singularities in generation of the FE mesh and numerical simulation.

2.3. Boundary conditions

It is well known that boundary conditions significantly influence the calculation results, especially, during viscous type flows. In our case, boundary conditions are formed to respond behaviour of the representative volume. We restrict ourselves that representative volume is located inside of the global volume, i.e. boundary conditions of the representative volume are not affected by the global boundary condition. Moreover, the influence of neighbour particles, as it used to be in the DE models, is also neglected. The above restrictions imply transversal incompressibility of the cylinder boundary and allow isolated treatment of the particles interaction. Consequently, only the global axial deformation of representative volume is allowed. It is clear, however, that using of incompressible boundary yields the upper bound of the stiffness of the interface layer. Our investigation confirms, that presence of the deformable boundary implemented by the thicker elastic layer up to infinity yields insignificant changes to local deformation and relatively small drop of the inter-particle stiffness.

Because of the axial symmetry the quarter of the half spheres will be considered. Geometry of the computation model with specified boundary conditions is illustrated in Figure 2. Generally, the boundary conditions of the cylinder are assumed to restrict motion of the material into normal outside direction, but can freely slide along the cylinder.

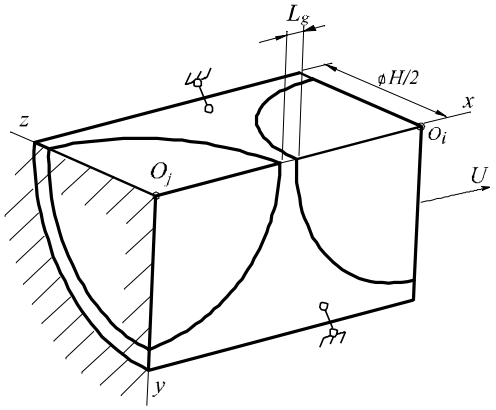

Fig. 2. Computational model of the normal interaction of particles with boundary conditions

Concerning model sections, the symmetric boundary conditions are specified on the vertical $O_i$xy and the horizontal $O_i$xz coordinate planes for both spherical particles and the interface material, i.e. their motion was restricted into normal directions and allows free sliding in tangential direction.

The kinematic boundary conditions were explored to describe the normal loading of the model during numeric simulations. The stretching load is imposed by moving particle i with respect to fixed particle j with the displacement value u_i. Actually, the values $u_i = U$ and $u_j = 0$ prescribed to all points of plane sections yO_ix and xO_jy including points on the interface material.

The bonded contact between spheres and interface is applied. For consideration of slip or debonding, the finer aggregates should be taken into account, and refined contact layer model is required [10, 22].

2.4. Viscoelasticity relations

Binder material between particles is assumed to be linear viscoelastic. It could be worth to notice that viscoelasticity is the property of materials that exhibit both viscous and elastic characteristics when undergoing deformation. Viscous materials exhibit time-dependent strain behaviour which is result of the diffusion of atoms or molecules inside a material.

It is common approach to present viscoelastic model as linear combinations of elastic and viscos components. In one-dimensional case, the elastic constitutive relationship between the stress σ and the strain ε, i.e. Hooke's law, can be regarded as linear spring with the elasticity constant equal to the elasticity modulus E of the isotropic continuum. The viscous components can be modelled as dashpots such that the linear stress σ and the strain rate $\dot{\varepsilon}$ relationship can be characterized by the viscosity coefficient of the material η while strain rate $\dot{\varepsilon} = d\varepsilon / dt$ is the time t derivative of strain.

Each of particular viscoelastic models differ in the arrangement of these elements. We employ the Maxwell model (Fig. 3) which defines the strain rate as a sum of elastic and viscous components [3, 6]:

$$\dot{\varepsilon}(t) = \frac{\dot{\sigma}(t)}{E} + \frac{\sigma(t)}{\eta} \tag{1}$$

When a material is put under a constant stress σ_0 the strain is obtained by integration of the rate. Finally, it yields two components

$$\varepsilon(t) = \frac{\sigma_0}{E} + \frac{\sigma_0}{\eta} t \tag{2}$$

The first, an elastic component occurs instantaneously, corresponding to the spring, and relaxes immediately upon release of the stress. The second is a viscous component that linearly increases with time as long as the stress is applied. In three-dimensions, constitutive relationship is defined in terms of stress and strain tensors, and can be expressed as a hereditary integral [3, 6]:

$$\sigma_{ij}(t) = E_0 \varepsilon_{ij} + \int_0^t E_t \frac{d\varepsilon_{ij}(\tau)}{d\tau} d\tau \tag{3}$$

It takes into account that the relaxation does not occur at a single time instant, but varies upon a time. Here, E_o is the constant instantaneous elasticity modulus. The transient part of the material is defined by E_t which is a function of the time t and reflects relaxation of the material stiffness. It is used to describe them with Prony series [15] as follows:

$$E(t) = E_o \left(1 - \sum_{m=1}^{M} \alpha_m^E e^{-\frac{t}{t_m}} \right) \tag{4}$$

Here, α_m^E and t_m are model parameters related to the mth component of the Prony series, while M is the number of Prony components in the model. Thereby, t_m is indicator of relaxation speed of the mth Prony component.

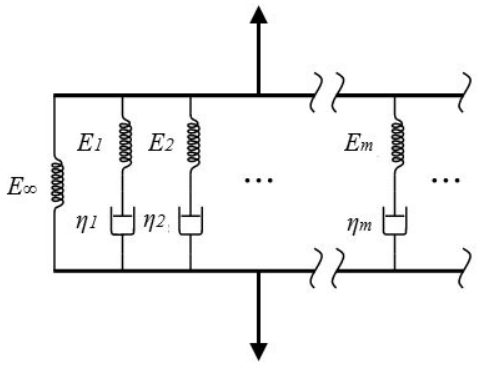

Fig. 3. Generalized Maxwell model for simulating viscoelastic behaviour

The stress tensor can be decomposed into the usual sum of volumetric and deviatory parts, σ_{kk} and $\hat{\sigma}_{ij}$, while strain tensor as ε_{kk} and $\hat{\varepsilon}_{ij}$, respectively. As a result, constitutive relationship can be decoupled, while each of the components is presented independently in the same manner as (3). Finally, volumetric and deviatory behaviours are described as follows:

$$\sigma_{kk}(t) = 3K_0 \varepsilon_{kk} + 3\int_0^t K_t \frac{d\varepsilon_{kk}(\tau)}{d\tau} d\tau \tag{5}$$

$$\hat{\sigma}_{ij}(t) = 2G_0 \hat{\varepsilon}_{ij} + 2\int_0^t G_t \frac{d\varepsilon_{ij}(\tau)}{d\tau} d\tau \tag{6}$$

Here, material properties are defined by is volumetric modulus K and is shear modulus G, respectively.

By assuming constant Poisson's ratio í purely elastic case is characterized by instantaneous parameters K_0 and G_0 expressed via elasticity moduli

$$K_0 = \frac{E_0}{3(1-2\nu)} \tag{7}$$

$$G_0 = \frac{E_0}{2(1+\nu)} \tag{8}$$

Time variations of $K(t)$ and $G(t)$ them may be described by Prony series according to (4).

2.5. Problem data

Numerical analysis of heterogeneous aggregates presented is accomplished on the scale of coarse aggregates defined hereafter as meso-scale. Problem data for normal interaction are chosen to imitate the behaviour of asphalt concrete presenting aggregate of stone particles embedded into bitumen binder.

The particles are assumed to be perfect spheres to simplify the calculation. They having radius R = 7.5 mm. The thickness of artificial outer layer tl is taken to be 1 mm. Thus, the diameter of the model cylinder (Fig. 2) is defined to be equal $H = 2(R + t_l) = 17$ mm, while its length L reflecting not only the particle's radius R but also the gap L_g, is variable parameter.

Mechanical properties of elastic particles are attributed to the features of granite [23]. The Young's modulus E is equal to $3 \cdot 10^{10}$ Pa while Poisson's ratio $\nu = 0.25$.

Viscoelastic properties of the binder material respond to the asphalt bitumen and were taken from [24]. They are sensitive to environment temperature and to loading rate. To simplify problem the values responding conditions of the standard Marshall test [25] and defined at fixed temperature equal to 60^{o} C and loading rate is 0.847 mm/s were considered in all examples below.

The Poisson's ratio is equal to 0.46 and indicates relatively high incompressibility. Time-dependent properties are constant throughout the volume. They are defined by constants of the Maxwell element. Here, time-independent elasticity constant E_∞ = 46 MPa. The values of constants α_m^E and t_m are given in the Table 1.

Table 1

Time-dependent properties of the viscoelastic materials related to Prony series

Component m	Factor α_m^E	Time t_m
1	0.902	0.637
2	0.072	6.175

3. THE FINITE ELEMENT MODEL

Simulation of the normal interaction of elastic spheres via viscoelastic interface was conducted by the Finite Element Method. Generation of the model and transient FE analysis was performed by using the FEM ANSYS 13 Workbench software [26].

3.1. Generation of the model

The model domain comprising a quarter of the cylinder shown in Figure 2 was investigated. Geometry of the FE model is defined parametrically and controlled by the basic parameters such as prescribed radius of the particle R and the variable parameter, i.e. the initial size of the gap between particles L_g. The tetrahedron type volume elements SOLID187 with 10 nodes were used for generation of the model.

The particles volume is described by coarsest mesh with the average element size equal to $0.1R$. The volume of the interface material is conditionally divided into two regions. The contact region between spheres is divided by the finest mesh with the average element size equal to $0.01R$ while the remainder region is $0.05R$ size. The quality of generated mesh was evaluated according to ANSYS requirements [26] by checking by skewness ratio of element.

Sample of, the total FE model consists of 19678 nodes and 9967 elements (Fig. 4). Model sizes, material properties and kinematic boundary conditions were defined in section 2.

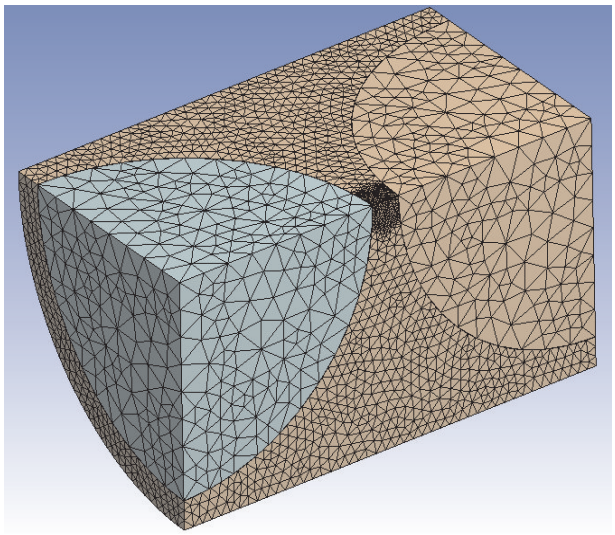

Fig. 4. Finite element mesh of the model domain

3.2. Characterisation of the model properties

Deformation behaviour of the softer interface is characterised by extremely large values of the local strains. Therewith, evaluation of them is important factor has to be conducted by modelling of mixtures. On the results of comprehensive review [10] it was concluded, however, that accurate analytical of solutions of the highly nonlinear problem are not available.

In opposite, the FE code ANSYS and the employed 3D finite element SOLID187 offer many possibilities in terms of various material models and problem formulations. It could be employed for simulating of physical and geometric nonlinearities. Large deflection approach, applicable to static and transient structural analysis, determines automatically whether the solver should take into account large displacements, large rotations and large strains.

The influence of geometric nonlinearity was studied by tracing incrementally the behaviour of the developed model in time. To evaluate particles interaction the geometrically induced loading history is defined as linear function of time while maximal displacement $U = 0.5$ mm is reached after 0.59 s. The sample having the initial gap $L_g = 0.5$ mm was examined.

Simulation results obtained are illustrated in Figure 5, where variations of the normal tension force F via displacement U incrementally are exhibited. The results of the viscoelastic model denoted by bold lines indicate drop of the material properties in time when compared to purely elastic case (thin lines).

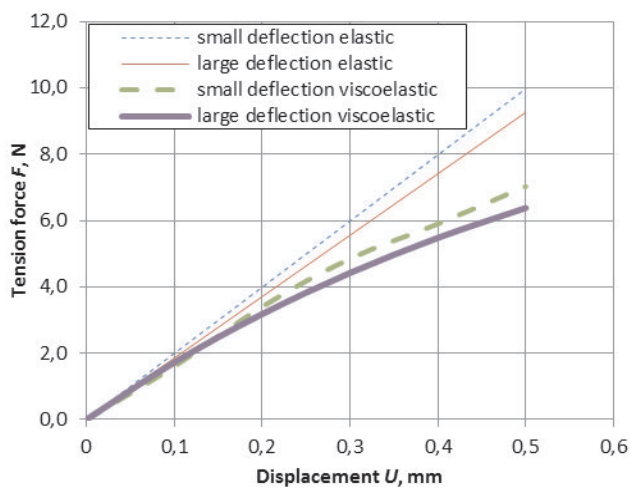

Fig. 5. Variation of the normal tension force via displacement for various models

As concerns nonlinearity, it are obvious that finite deflection approach results of which is denoted by solid lines indicates relatively higher displacement values. More precise evaluation shows that neglecting of geometrical nonlinearity overestimates displacement and stiffness. Our sample shows that at the load level F = 6.0 N artificial increase of the inter-particle displacement reaches 5% for elastic case and 9% increase for viscoelastic case.

In summary, for the future calculations the large deflection model is preferable.

4. INVESTIGATION OF THE INFLUENCE OF THE INTER-PARTICLE GAP

4.1. Basic statements

Empirical and theoretical investigations show influence of the inter-particle interface material. Current presentation is aimed to influence of the initial inter-particle gap under tension load. The size of the gap means the smallest distance between two surfaces of interacting spheres. The problem is considered numerically, while the concept of the finite element model, along with basic data is described in pervious sections. The more realistic large displacement model is exclusively used in simulations. The loading is imposed by moving the spheres in opposite direction until prescribed displacement U = 0.5 mm.

Four cases of the model domain with various gap sizes and four finite element models were generated, respectively. The selected values of the gap size L_g equal to 0.1. 0.5, 1.0 and 1.5 mm corresponding to 0.013R, 0.066R, 0.133R and 0.2R, respectively, were considered in the numerical experiment. For further reduction of gap size properties of bitumen film it has to be taken into account.

4.2. Evaluation of the tension force

The tension behaviour of the interface material was basically examined by considering the normal force. The value of the force is extracted from the results of FE calculation. It is obtained as a reaction force of the sphere due to their pulling motion.

Two limit cases corresponding to the sizes of inter-particle gap L_{g1} = 0.1 mm and L_{g4} = 1.5 mm, respectively, were selected for illustration of the force calculation methodology while the results of viscoelastic samples are examined in details.

Tension force presents resultant contribution of the normal pressure and the tangential traction (frictional pressure). The nature of the force is basically predicted by considering pressure distribution on the sphere. Two different cases of pressure distributions are illustrated in Figure 6. The negative values mean tension (suck) pressure given in Pascal's.

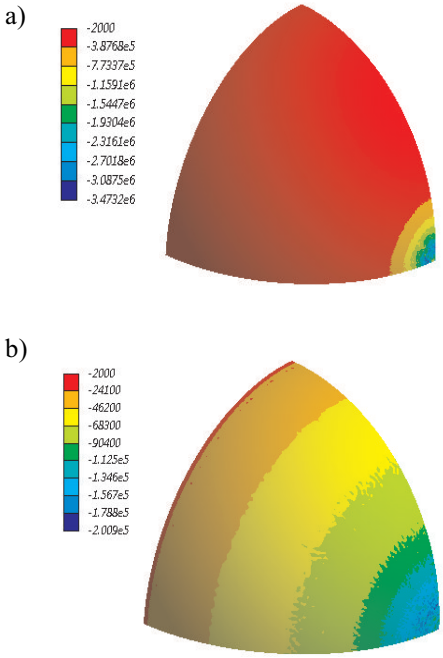

Fig. 6. Contour plot of the pressure on the sphere: a) L_{g1} = 0.1 mm; b) and L_{g4} = 1.5 mm

The pressure colour analysis indicates that for smaller gap (Fig. 6a) the highest values of pressure p_1(r) varying in the range between $p_{1,\max}$ = 3.47 MPa and 1.16 MPa are concentrated within the small circle having radius $r \approx 0.1R$. The of distribution pressure p_4(r) in another sample is much different (Fig. 6b). it has a gradual decreasing character while the maximal pressure $p_{4,\max}$ = 0.2 MPa is almost 18 times lower. Another observation is that values of the tangential traction are in average about 10 times lower.

Calculation results yielded two force values F_1 = 11.42 N and F_4 = 4.35 N, respectively. Additional information could be extracted by considering accumulative nature of the normal force. Radial variation of the relative accumulated forces $F_a(r)/F$ against the particle radius r/R ($0 \le r/R \le 1$) is illustrated in Figure 7.

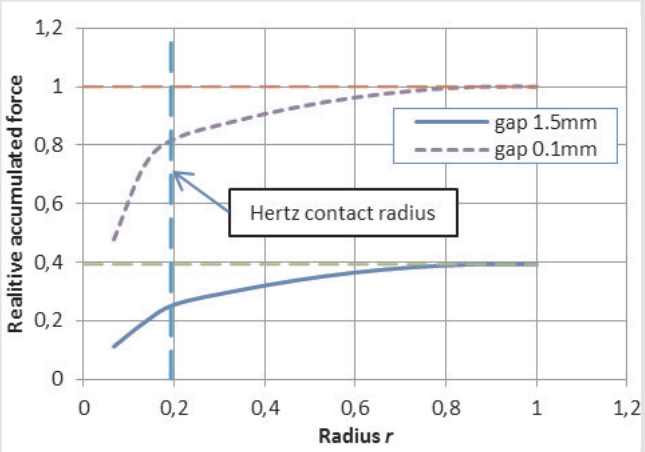

Fig. 7. Variation of relative accumulated resultant force across the sphere radius. For various gaps

It is ease to detect from the graph that the obtained relationship between resultant forces $F_4/F_1 = 0.39$ indicates significant drop of the force with increase of the gap size. On the other hand, it could be state that the above ratio is much lower them the ratio of maximal pressures $p_{4,\max}/p_{1,\max} = 0.058$, which indicates different character of the pressure profiles.

4.3. Illustration of the space dependent properties

Several aspects are studied below. We try to separate the space defined effects influenced by the gap size and the time-dependent effects obtained by viscoelastic results.

A general tendency related to the gap size was already observed in earlier discussion indicating that the magnitude of the force and stiffness significantly varies with decrease of the initial distance between the aggregate spheres, i.e. the smaller the initial distance, the bigger the force needed to withdraw the sphere.

The influence of the initial gap was extracted by processing simulation results and demonstrated separately. Variations of the force values at the end of the loading at highest elongation period against the relative size L_g/R of the gap are illustrated in Figure 8, while variations of the secant stiffness are given in Figure 9.

Here, viscoelastic behaviour is illustrated by dashed lines, while elastic results denoted by solid lines are presented for the sake of comparison. There, force and displacement are scaled with respect to interface properties and presented by dimensionless parameters $f = F/E_0 L_g R$ and $u = U/L_g$, respectively.

Differences in deformation behaviour during interaction under tension may be considered by exhibition of the state variables. Illustrative sample is given in Figure 10, where contour plot of the maximal principal (tensile) logarithmic strain is plotted the central sections. Simulation results indicate extremely high values of strains in interface layer which coincide with those obtained by the other researches [10].

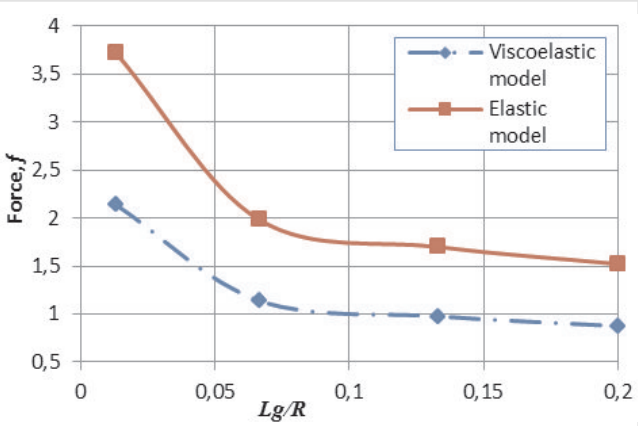

Fig. 8. Variation of the normal interaction force values against the size of the initial gap for various models

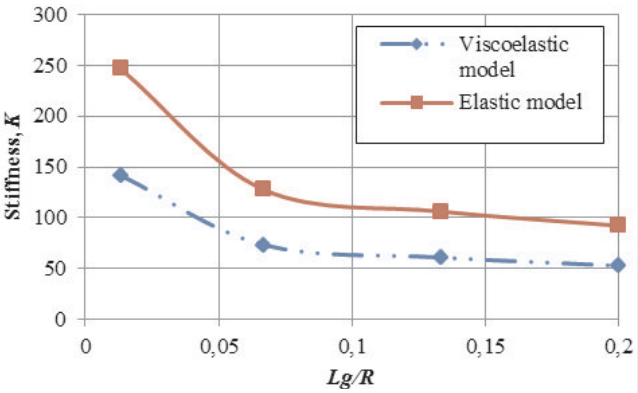

Fig. 9. Variation of the normal stiffness values against the size of the initial gap for various models

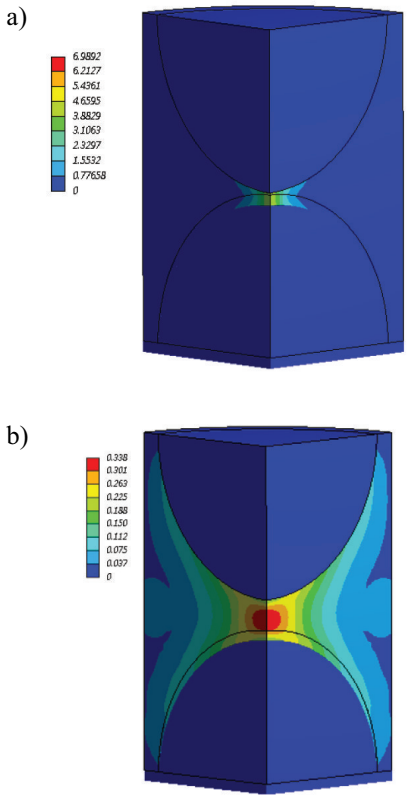

Fig. 10. Variation of maximum Principal Elastic strain: a) $L_g = 0.1$ mm; b) $L_g = 1.5$ mm

The pictures also show differences in the behaviour interface material. For the small gap, the tension is characterised by uniaxial stretching concentrated within the small cylinder. The increase of the gap size that that highest strains values occur in the middle of the gap between two particles.

4.4. Investigation of temporary behaviour

To evaluate temporary behaviour numerical results obtained by applying viscoelastic approach were additionally examined. Original simulation results are presented in terms of the normalised dimensionless force–displacement relationship. The curves illustrated in Figure 11 reflect typical character of viscous models.

In order to describe the viscoelastic behaviour, a general approach [27] considers the time-dependent force and the displacement relation $F(U(t))$ functions in a form of very complex function $F(t) = G(U, t)$. It is used to name this function as relaxation function.

In the case linearity the relaxation function becomes only function of time $G(t)$. In our case, geometrical nonlinearity was imposed. To illustrate influence of the nonlinearity, the secant stiffness is extracted frown the curves in Figure 11 and, after scaling, is defined in the nondimensional forms. The obtained results are shown in Figure 12. Actually time variation of the stiffness may be interpreted s relaxation functions.

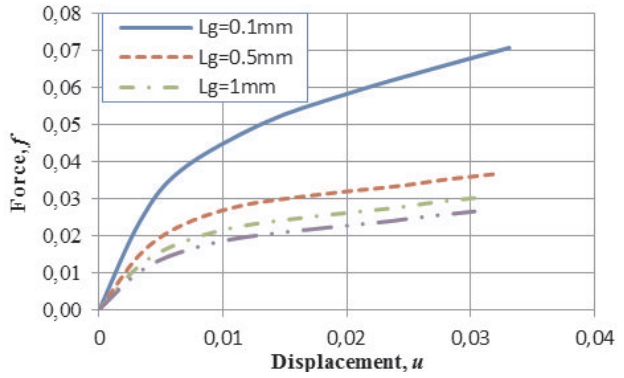

Fig. 11. Calculated normalised force displacement relationship under tension for various values of the size of initial gap

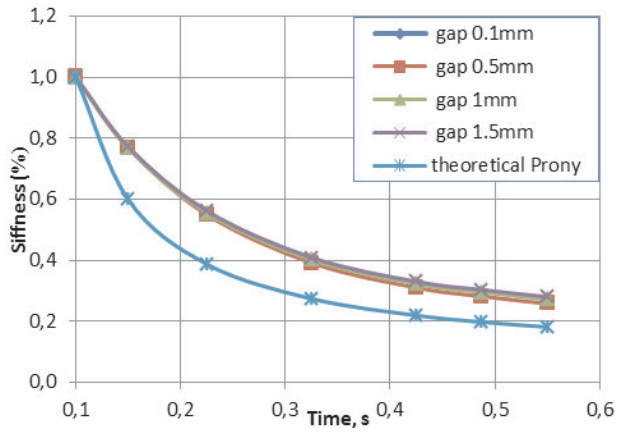

Fig. 12. Variation of relaxations functions for various sizes of the gap

The results exhibit clear similarity of curves what means that influence of the gap has predicted by the geometry properties and the space resolution but this factor has minor influence to viscous properties. Dimensionless relaxation function for material defined by Prony series (4) is also presented for the sake of comparison. Results show slower relaxation of the interaction behavior when compared to the local relaxation of the material.

4.5. Discussion on the influence of the size of the gap

Summarizing results of the finite element simulation of the normal interaction of elastic particles in the confined viscoelastic solid under tension some important observations could be pointed out. Relaxation curves (Fig. 12) demonstrate that the size of interface gap has small contribution to temporary variation of stresses and strains. Consequently, similarity of non-dimensional relationships obtained after scaling should be valid independently on material model.

Investigation particle's interaction via interface on the basis of purely continuum approach indicated existence of two different states separated by critical value of the gap size. Considerable stiffening of in constitutive behaviour of the matrix material is indicated below this size.

Our manifest suggests that this critical size is relevant to the Hertz contact radius obtained at the given load level $F(t)$. Defining contact radius by classical expression [27].

We obtained $a = 0.19R$. Referring variation of accumulated force given in Figure 7. We can find that major part of the resultant force is accumulated by the central part of the sphere within this radius.

Required force employed for interaction analysis could be chosen from the above results. Additionally, the circle with radius $0.2R$ yields $0.83F_1$ and $0.59F_4$. This means that radius of the representative volume and incompressible boundaries are applicable for simulation and has minor influence to the final results.

In the limit when gap size approaches zero $L_g \to 0$ we obtain the Hertz force $F_H = 9.28$ N [27].

$$F_h = \frac{4}{3} \cdot E^* \cdot \sqrt{R} \cdot u^{\frac{3}{2}} \tag{9}$$

were:

F_h – Hertz contact force,
E^* – contact elastic modulus;
R – particle radius,
u – indentation deep.

In the limit case the interaction may be interpreted as contact of two particles with parallel bond as it is used in bonded granular materials [27]. However, sophisticated microstructure models will be required to reflect influence of the finer particles in interface for real asphalt mixtures.

Regarding increase above the critical size of the gap, contributions of particles contact drops and infuse of material increases. The pressure will form decay zone between

particle and this zone will separated into two indicating motion of the single spheres. Qualitatively, pressure distributions evaluation of be alternatively define by fluid models [28].

5. CONCLUSIONS

Final conclusions are formulated as follows:

- Since interface material possesses observable changes of the geometry, influence of the geometric nonlinearity was evaluated by comparing linear and large deflection models. Observable up to 5÷9% difference of normal force was found, therefore, nonlinear large deflection model is recommended for interaction analysis.
- Strain analysis shows that deformability of particles is negligibly small and could be neglected in the computational models. Consequently, particles could be presented by rigid surface, thereby, simplifying computational model and reducing the size of the model.
- Results clearly demonstrate influence of the viscosity of interface solid. For normal displacement of particles equal to 6.6% of particle radius R, yields reduction of the interaction force up to 56.7% when compared to purely elastic properties.
- Investigation of the size of initial inter-particle gap on the basis of purely continuum approach confirmed presence of interface layer around stiffer particle. Reduction of the inter-particle below critical size approximately equal to 0.066 of particle radius yields significant increase of interaction stiffness.
- It was shown that critical size is predicted by the geometry and is not sensitive to temporary behaviour. Future research is required to examine this effect regarding microstructure of interface.

References

[1] Alavi A.H., Ameri M., Gandomi A.H., Mirzahosseini M.R. 2011, *Formulation of flow number of asphalt mixes using a hybrid computational method*. Construction and Building Materials, 25, 3, pp. 1338–1355.

[2] Sivilevičius H., Podvezko V., Vakrinienė S. 2011, *The use of constrained and unconstrained optimization models in gradation design of hot mix asphalt mixture*. Construction and Building Materials, 25, 1, pp. 115–122.

[3] Schapery R.A. 1969, *On the characterization of nonlinear viscoelastic materials*. Polymer Engineering and Science, 9, 4, pp. 295–310.

[4] Schapery R.A. 2000, *Nonlinear viscoelastic solids.* International Journal of Solids and Structures, 37, pp. 359–366.

[5] Tashman L., Masad E., Little D., Zbib H. 2005, *A microstructure-based viscoplastic model for asphalt concrete*. International Journal of Plasticity, 21, 9, pp. 1659–1685.

[6] Park S.M., Kim Y.R., Schapery R.A. 1996, *A viscoelastic continuum damage model and its application to uniaxial behaviour of asphalt concrete*. Mechanics of Materials, 24, pp. 241–255.

[7] Schapery R.A. 1999, *Nonlinear viscoelastic and viscoplastic constitutive framework for the nonlinear viscoelastic behavior of pultruded composite materials*. International Journal of Fracture, 97, pp. 33–66.

[8] Mun S., Lee S. 2010, *Determination of the fatigue-cracking resistance of asphalt concrete mixtures at low temperatures*. Cold Regions Science and Technology, 61, pp. 116–124.

[9] Krishnan J.M., Rajagopal K.R. 2005, *On the mechanical behavior of asphalt*. Mechanics of Materials, 37, 11, pp. 1085–1100.

[10] Liu Y., You Z., Dai Q., Mills-Beale J. 2011, *Review of advances in understanding impacts of mix composition characteristics on asphalt concrete (AC) mechanics*. International Journal of Pavement Engineering, 12, 4, pp. 385–405.

[11] Kose S., Guler M., Bahia H.U., Masad E. 2000, *Distribution of strains within asphalt binders in hma using image and finite-element techniques*. Transportation Research Record 1728, Transportation Research Board, Washington, D.C., pp. 21–2.

[12] Dai Q. 2011, *Two- and three- dimensional micromechanical viscoelastic finite element modelling of stone- based materials with X- ray computed tomography images*. Construction and Building Materials, 25, pp. 1102–1114.

[13] You Z., Adhikari S. 2008, *Models for asphalt mixtures using X-ray computed tomography images*. International Journal of Pavement Research and Technology, 1, 3, pp. 94–99.

[14] Sadd M.H., Dai Q., Parameswaran V., Shukla A. 2004, *Microstructural Simulation of Asphalt Materials: Modelling and Experimental Studies*. Journal of Materials In Civil Engineering March/April, pp. 107–114.

[15] Mo L.T., Huurman M., Wu S.P., Molenaar A.A.A. 2008, *2D and 3D meso-scale finite element models for ravelling analysis of porous asphalt concrete*. Finite Elements in Analysis and Design, 44, 4, pp. 186–196.

[16] Guddati M.N., Feng Z., Kim Y.R. 2002, *Toward a Micromechanics-based Procedure to Characterize Fatigue Performance of Asphalt Concrete*. Transportation Research Record, No. 1789, Transportation Research Board, National Research Council, Washington, D.C., pp. 121–128.

[17] Sadd M.H., Dai Q.L., Parameswaran V., Shukla A. 2004, *Simulation of asphalt materials using a finite element micromechanical model and damage mechanics*. Journal of Transportation Research Record, 1832, pp. 86–94.

[18] Bahia H., Zhai H., Bonnetti K., Kose S. 1999, *Nonlinear viscoelastic and fatigue properties of asphalt binders*. Journal of Association of Asphalt Paving Technologists, 68, pp. 1–34.

[19] Dai Q., Zhanping Y. 2007, *Prediction of Creep Stiffness of Asphalt Mixture with Micromechanical Finite-Element and Discrete-Element Models*. Journal of Engineering Mechanics, 133, 2, pp. 163.

[20] Jiang M.J., Yu H.S., Harris D. 2006, *Bond rolling resistance and its effect on yielding of bonded granulates by DEM analyses*. International Journal.

[21] Chareyre B., Cortis A., Catalano E., Barth_el_emy E. 2011, *Pore-scale Modeling of Viscous Flow and Induced Forces in Dense Sphere Packings*. Soft Condensed Matter arXiv:1105.0297v2

[22] Zhu X., Yang Z., Guo X., Chen W. 2011, *Modulus prediction of asphalt concrete with imperfect bonding between aggregate-asphalt mastic*. Composites: 42 1404-1411

[23] Matweb [Online] http://www.matweb.com/ [cited 04 Feb. 2011LST EN 12697-34:2004.

[24] Huurman M., Woldekidan M.F. 2007, *[online]. LOT, Mortar response; measurements, test interpretation and determination of model parameters*. TUD-report_7-07-170-3.pdf [cited 11 September 2010]. Available from Internet: http://citg.tudelft.nl/

[25] Bituminous mixtures - Test methods for hot mix asphalt - Part 34: Marshall Test. Date issue 2004-10-15. Lithuanian Standards Board, 2004.

[26] Ansys 2010. version 13 program manual.

[27] Johnson K.L. 1987, *Contact mechanics*. Cambridge University Press.

[28] Navardi S., Bhattacharya S. 2010, *Axial pressure- difference between far-field across a sphere in viscous flow bounded by a cylinder*. PHYSICS OF FLUIDS 22 1033505, p. 1–17.